Seventh Canadian Masonry Symposium
McMaster University
Hamilton, Ontario
June 4-7, 1995

NUMERICAL SIMULATION OF TALL MASONRY CAVITY WALLS TESTED UNDER ECCENTRIC LOADING

R. Wang[1], A.E. Elwi[2], and M.A. Hatzinikolas[3]

ABSTRACT

This paper presents the results of the second phase of an ongoing investigation into the behavior of cavity masonry walls constructed with concrete block, brick veneer and shear connectors. In the first phase, a test program has been conducted on tall cavity walls under eccentric axial forces. In this phase a nonlinear finite element analysis model is developed to simulate the database of existing test results. The model represents all components of the cavity wall, the reinforced concrete block back-up wythe, the brick veneer and the shear connectors. It accounts for the nonlinear material behavior of all components as well as the large rotation small strain characteristics of the deformation. The numerical analysis results are successfully compared with a number of test results. The simulation offers insight into the mode of failure, in particular for walls with high eccentricity ratios.

INTRODUCTION

At present the design of masonry cavity walls subject to eccentric axial compressive forces is difficult due to inadequate information on the evaluation of their flexural rigidity and the contribution of the veneer to the axial load capacity. To fully understand the behavior of masonry cavity walls, a large number of wall tests are required in order to incorporate a wide range of performing parameters affecting wall behavior. However, such a fully experimentally based investigation is too expensive and time consuming to be feasible in practice. A small number of full scale tests are critical, however, to provide reliable information for assessing the behavior of any system. In this work, the experimental

[1] Research assistant, Dept. of Civil Engineering, University of Alberta
[2] Professor of Civil Engineering, University of Alberta, Edmonton, Alberta, T6G 2G7.
[3] Executive Director, Canadian Masonry Research Institute, Edmonton, Alberta.

database obtained at the University of Alberta consists of four plain cavity walls and three reinforced cavity walls tested by Goyal et al.(1993) and a more recent series of nine reinforced cavity walls tested by Wang et al. (1995).

In order to expand the database a numerical analysis model can be used to investigate the full range of parameters not covered by the tests. The performance of this model must, first, be verified against the test results in order to develop confidence in the results and to develop an insight into the mode of failure. This paper presents a simple and efficient nonlinear finite element model developed to complement the experimental work. The model was implemented in the general purpose finite element program ABAQUS(Hibbitt et al. 1994). The model accounts for both the material and geometrical nonlinearity aspects of the tests. The model is then used to simulate the results of the most recent Wang et al.(1995) series. This series consisted of nine 5.29 m high walls each wall was constructed with a 200 mm backup concrete block wythe partially grouted and reinforced and a 90 mm thick burnt clay brick wythe. The two wythes were connected with a constant arrangement of shear connectors (Wang et al. 1995). The finite element analysis results, specifically, the load-deflection response curves and critical loads are compared to the test results and the failure modes are discussed.

NUMERICAL MODEL

Finite Element Mesh

Masonry walls subjected to combined axial load and out-of-plane bending moment are usually designed to span vertically. Such walls work essentially as columns with uniformly distributed deflection along the width of the wall. Since Poisson's ratio properties in masonry walls are not clear, plain strain response was neglected, and plane stress conditions were assumed. These walls could be modeled as a two dimensional continuum or as a beam assembly. The model presented herein is a beam model with the different components modeled along their centerlines.

Two reasons were considered when selecting a beam element model instead of a two-dimensional plane stress element model. First, the beam element is simpler with fewer nodes in an element which is more suitable to model large dimensional structures. Second, we are more interested in its overall behavior - the stiffness and strength for instance, of the masonry walls under consideration, rather than in the local distribution of the stresses.

There are several types of beam elements available in ABAQUS. The 3-node quadratic beam type element, B22, was selected for masonry assemblages. This type of element uses Timoshenko beam theory which takes into account the transverse shear deformation of cross-section. Hence, the deformed cross-section may not remain normal to the beam axis. Such an assumption is consistent with the case of masonry assemblages under out-of-plane bending where the transverse shear deformation is significant (Essawy et al. 1985). Unlike the response to axial and flexural loads, the transverse shear deformation is treated in ABAQUS as a linear elastic response.

To model the shear connectors, a special type of element- 3-node quadratic beam elements with hybrid formulation B22H was used. This is because the shear connector is a very short element. It exhibits very large stiffness to the axis of bending. It was found from analysis that a beneficial effect is achieved by using hybrid elements which treat the axial and transverse shear forces as independent degrees of freedom. The shear connectors were modeled with an elastic perfectly plastic von Mises material model.

Microscopic vs. Macroscopic Models

A microscopic model has been developed and tried in this research project initially. The model separately considered each mortar joint and each unit. There was no interface element between the mortar joint and unit. The mortar tension failure mode was based on the debonding limiting stresses between mortar and unit. It was found that analytical results based on this model were not satisfactory. In the authors opinion, this model was unable to simulate the crack propagation between elements after debonding. The discontinuity of deformation between a debonded mortar element and a unit element caused numerical solution problems. Some improvement to this model may be achieved by adding interface elements between joints and units (Lotfi, et al. 1994). However, adding interface elements is expensive since it would make the number of elements which are already quite large even larger with no guarantee that satisfactory results could be obtained.

For the above reasons, a macroscopic model was finally chosen. In this model, the wall is descretised into finite elements with no particular attention given to the position of mortar layers. Debonding would most probably occur within an element which could be modeled as a crack and allowed to propagate as a crack. Properties of masonry assemblage as a whole, that is, the properties of masonry prisms could thus be used instead of the different properties of each individual material component. The weakness of the mortar layer in tension was considered by using the bond strength as the tensile strength between concrete masonry units and mortar joints as well as between brick units and mortar joints respectively. Detailed material properties will be discussed in the next section.

Figure 1 shows the proposed finite element mesh. Where, the concrete masonry wythe is simply supported with a hinge at the bottom and a roller at the top. A relatively stiff element was used to model the steel angle at the bottom of the brick masonry wythe. One end of this element is fixed to the bottom of the concrete masonry wythe and the other end is connected to the brick masonry wythe by a two-node constraint equation. The two nodes are overlapped at one point by a constraint equation which allows horizontal movement while constraining the vertical movement between the steel angle element and brick masonry wythe to be equal. Hinges were used to model the connection between the shear connector plates and the V-ties while fixed end conditions were used to model the joints between the connector plates and the concrete masonry elements as well as between the V-ties and the brick masonry elements.

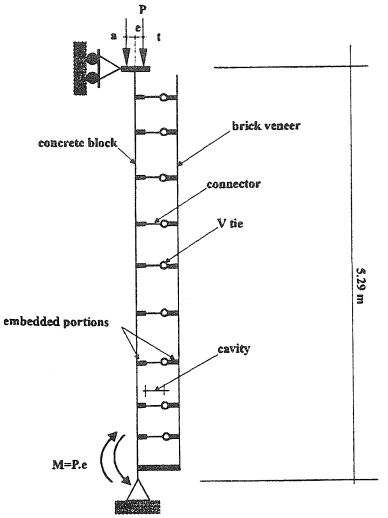

Fig. 1 Finite element mesh

The stiffness and the cross-sectional area of the portions of the shear connector plates and V-ties embedded within the masonry wythes were modeled with values higher than those of the connectors or V-ties themselves. The ratios of properties between embedded and outstanding parts were one hundred for moment of inertia and ten for cross-sectional area. A larger ratio was selected for the bending stiffness because embedment contributes more to the stiffness than to the cross-sectional area of shear connectors. The selection of those ratios was semi-empirical since little information was available from previous research. Papanikolas et al.(1991) assumed infinitely large stiffness and cross-sectional area for the embedded part of connectors in their linear elastic model of these walls.

Material and Parameters

In the elastic range, the masonry assemblage was modeled as an isotropic elastic material. The Young's modulus of both concrete masonry and brick masonry were based on the average prism test values. These Young's moduli and Poisson's ratios are listed in Tables 1.

Beyond the elastic range, the material option *CONCRETE in ABAQUS was used to model masonry assemblages. This option provides a smeared crack propagation simulation. The cracking failure criterion is defined by a "crack detection surface" which is a function of the principal stresses. Once the stress state reaches this surface cracking is initiated. The presence of cracks will be reflected in the constitutive calculation at related integration points. That is, the stress and material stiffness at that integration point will be changed. Since at each integration point, different constitutive values may be used, the crack propagation from point to point can be simulated.

In order to use this material model, several material properties have to be defined. First, the uniaxial compressive stress-strain relationship. A simplified curve with several straight line segments was selected in which the ascending part was defined by prism test results and the descending part was obtained according to the proposed curve by Atkinson and Yan (1990). This simplified curve was used both for concrete masonry and for brick masonry with different control parameters, f'_m, which were obtained from tests.

For masonry in tension, as mentioned above, the bond strength between the units and mortar layers were used as tensile strength since in most cases masonry experiences tensile failure by debonding of mortar and units. The tensile strength values as defined above are listed in Table 1 where ratios of these uniaxial tensile strengths to the corresponding uniaxial compression strengths are also listed as required by ABAQUS.

Table 1 Properties of concrete block masonry

	Material properties (a)	Values used (b)	(b)/f'_m (c)
Concrete block	Modulus of elasticity	13920 MPa	721.2
	Poisson's Ratio	0.2	N / A
	Compressive strength, f'_m	19.3 MPa	N / A
	Tensile (bond) Strength	0.56 MPa	0.029
Brick Veneer	Modulus of elasticity	6536 MPa	361.0
	Poisson's Ratio	0.2	N / A
	Compressive strength, f'_m	18.1 MPa	N / A
	Tensile (bond) strength	0.63 MPa	0.035

Another category of parameters defines the phenomenon of tension stiffening which reflects the post-cracking behavior between the cracks. Unfortunately, to the best of our knowledge there is no such information for masonry. A reasonable way of estimating the tension stiffening effect in reinforced masonry structures is to compare it with reinforced concrete structures. In reinforced concrete structures, the tension stiffening effect is a function of the reinforcement ratio, the bond strength between rebar and concrete, as well as the finite element mesh. In reinforced masonry structures, beside those mentioned above, the grout fill, in authors' opinion, has a significant effect on tension stiffening behavior. This is because the grout fill bonded with rebar is a continuos member from top to bottom of the wall. Moreover, the tensile strength of grout material is much higher, usually more than five times that of the bond strength of masonry. Thus, once the debonding occurs between a unit and a mortar joint, the grout fill together with rebar will act as a stiffener to resist the propagation of debonding. Therefore, the complete debonding of that joint is delayed. This effect needs to be quantified in future research. At present, the tension stiffening is modeled here with the descending part of the stress strain curve in tension. The total strain corresponding to the stress ranging from failure to zero

was selected as 4.3×10^{-3}. Figure 2 shows the complete stress-strain curves used in this study.

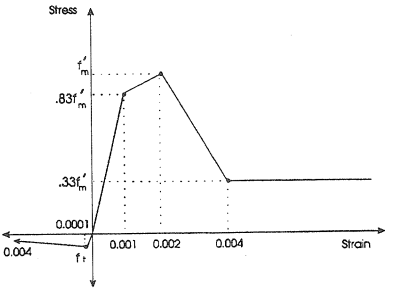

Fig.2 Stress strain curve for the block material

In an earlier phase of the project an equivalent stiffness *EI* has been derived which converts the hollowed connector plate into a plate with a solid cross-section. These values of EI were used to model the connector behavior. The modulus of elasticity, E , of the connector plate was selected as 200 GPa. The cross-section of connector plates was sized so that the products of moment inertia of the cross-section and the modulus of elasticity equaled the desired *EI* value. The equivalent cross-sectional areas of the shear connectors were defined according to the load-displacement response of the shear connector tests. A value of yield strength of the connector was defined as a nominal strength such that the capacities of the connectors based on the equivalent cross-section approach to the ultimate capacity of the connector under a combined load condition. These values are listed in Table 2.

Table 2 Properties of the connector element

Material properties	75 mm connector	100 mm connector
Modulus of elasticity, E	200 MPa	200 MPa
Nominal yield strength, f_y	300 MPa	300 MPa
Area/connector	2.96 mm^2	1.83 mm^2
Moment of Inertia/connector, I	14030 mm^4	9550 mm^4

Analysis Procedure

The loading procedure was carried out incrementally in several stages using a load control solution strategy with a standard Newton-Raphson iterative procedure. Before reaching the ultimate load point, the solution strategy switched to a modified Riks algorithm to obtain the ultimate load P_u and to proceed into the post-bucking load-displacement response.

Another aspect of the analysis is the treatment of the buckling behavior of the shear connectors. Once a connector is buckled, the load on that connector will be redistributed among other connectors. This phenomenon was modeled with ABAQUS's option *MODEL CHANGE in which an element that is no longer effective is removed. It was assumed that successive failure would occur in a row of connectors if only one buckled. Thus, the removal of a connector element means that an entire row of connectors, which in this analysis contains two or three connectors, is removed.

SIMULATION OF TEST RESULTS

All tests here were conducted on walls made with 200 mm blocks with a variety of end conditions and eccentricities. The eccentricities referred to here are measured from the centroidal axis of the block wythe. Table 3 summarizes the parameters of the test specimens as well as the results of both test and analysis.

Table 3 Summary of specimen properties and comparison with test results

Wall	C^* (mm)	e_1/e_2	e^{**}	ecc. type	Slenderness ratio	P_u Analysis (kN) (a)	P_u Test (kN) (b)	(a)/(b)
W1	75	1	*t/3*	a***	27.8	447.8	451.0	0.993
W2	75	0	*t/3*	a	27.8	938.0	818.5	1.146
W3	75	0	*t/3*	t****	27.8	662.0 (913.6)	651.9	1.015 (1.401)
W4	75	-1	*t/3*	N/A	27.8	1198.0	1200.1	0.998
W5	75	0	*t/3*	a	27.8	938.0	815.5	1.150
W6	75	1	*t/2*	t	27.8	236.4	251.4	0.940
W7	100	1	*t/3*	t	27.8	424.4	424.0	1.001
W8	75	1	*t/2*	a	27.8	168.7	166.0	1.016
W9	75	-1	*t/2*	N/A	27.8	738.0	822.9	0.897

* *C: cavity;*
** *e: eccentricity*
*** *a: away from veneer*
**** *t: towards veneer*

Group 1, Loading with $e_1/e_2 = 1$

This group consists of specimens W1, W6, W7 and W8. Specimens W1 and W8 had 75 mm cavities, were loaded with eccentricities away from brick veneer. However, W1 was loaded with an eccentricity $e=t/3$ while W8 had $e=t/2$. Specimens W6 and W7 were loaded towards veneer but the first had a 75 mm cavity and eccentricity of $t/2$ while the

second had a 100 mm cavity and a *t/3* eccentricity. Here "*t*" is the thickness of the block wythe which is constant at 190 mm.

Figures 3a, b, c, and d show the mid-height load-displacement responses of specimens W1, W7, W6 and W8, respectively, obtained from the analysis and from the test. It can be observed that the model performance is satisfactory since it reproduces most characteristics of the test curves. Specifically, the ultimate load P_u from analysis is consistent with that obtained in the test and the deformation of the wall obtained from analysis has good agreement with that obtained from the test even into the post-cracking range and the post-ultimate range.

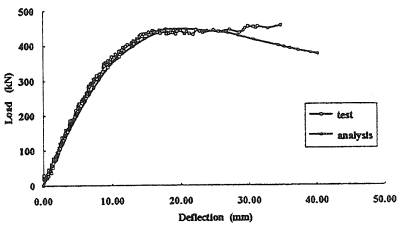

(a) Wall W1

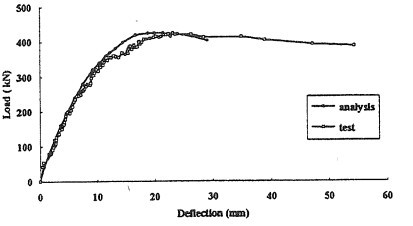

(b) Wall W7

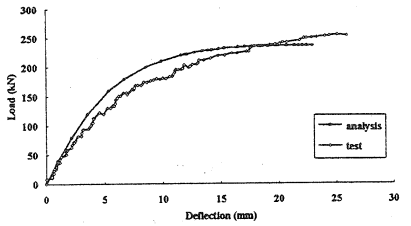

(c) Wall W6

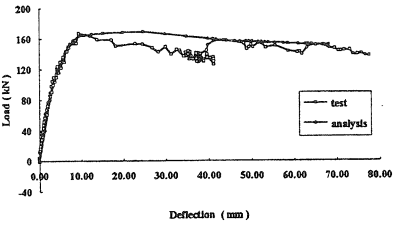

(d) Wall W8

Fig. 3 Mid height load displacement response for Group 1 (e_1/e_2=1)

It seems that the simulation of W6 response overestimates the cracking strength and underestimates the post-cracking capacity. Those differences may result from a number of reasons. The variation in the properties of masonry materials is high, especially the high variation in the bond strength between masonry units and mortar joints. Since specimen W6 was subjected to a load with large eccentricity (90 mm), the cross-section of the wall was subjected to a high strain gradient. Such a strain gradient may affect the tension stiffening behavior. That effect was considered constant in the analysis. Considering the two conditions, the small discrepancy between the analysis and test is understandable and acceptable.

It was found in the analysis of W8 that the shear connectors at the top of the specimen reached their ultimate load capacity and buckled. Those connectors were removed from

the wall for the subsequent load steps using the procedure described earlier. Both the ultimate load and the deflection history have been well predicted by the analysis.

Group 2, Loading with $e_1/e_2=0$

This group consists of two specimens W2 and W3. Both had 75 mm cavities and were loaded with an eccentricity of $e=t/3$ at the top of the wall and zero at the bottom. Specimen W2 was loaded away from the veneer while specimen W3 was loaded towards the veneer. Figures 4a and b show the numerical analysis and the test responses for specimen W2 and W3, respectively.

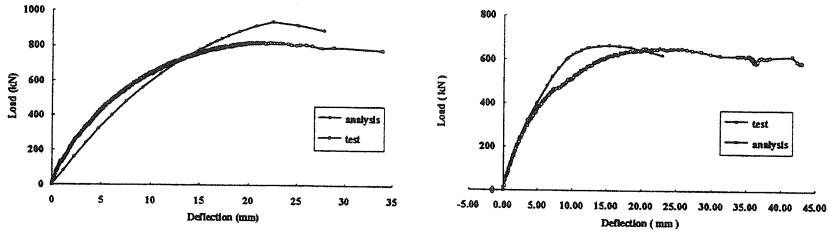

(a) Wall W2 (b) Wall W3

Fig. 4 Mid height load displacement response for Group 2 ($e_1/e_2=0$)

For specimen W2, the analysis overestimates the ultimate load capacity by fifteen percent. Again, the variation in the material properties and in the estimation of post-cracking strength may explain the discrepancy in the response.

For specimen W3 a lower load capacity was observed in the test than expected (Wang et al. 1995). Therefore, two sets of material properties were used to obtain two parallel numerical responses . In one set, average material properties obtained from prism tests were used as were the cases of other specimens. It was found that the analysis result corresponding to this set of material properties overestimates the ultimate load capacity P_u by 40 % (the bracketed values in column a Table 3). In the other set, a lower compression strengths $f'_m \approx 0.7\, f'_{m\ average}$ was selected both for concrete block masonry and for brick masonry. The corresponding tensile strengths were also changed with the same ratio. The numerical response based on this set of material properties agrees well with the test curve on the initial part of deflection and on ultimate load capacity.

Group 3, Loading with $e_1/e_2=-1$

This group consists of specimens W4 and W9. Both had 75 mm cavities and were both loaded with opposite eccentricities at the two ends of each specimen causing the walls to deflect in double curvature. The loading eccentricities for specimens W4 and W9 were $t/3$ and $t/2$ respectively.

Since both the initial conditions and the unwinding phenomenon have effects on the deflected shape of specimens with double curvature, relative displacement between upper and lower curves are plotted instead of deflection at one point.

Figure 5 shows the relative displacement between nodes at elevations of 0.85 m and 4.4 m from the bottom of the specimens W4 and W9 obtained from the analysis and the test. In the analysis, the loading steps were designed to follow the loading procedure of the test exactly. In the test, the failure started from the outer face-shell of the top block of concrete masonry wythe where the top concrete block masonry reached its prism compression strength. The failure mode and the locations of failure detected by the analysis were the same as those observed in the test.

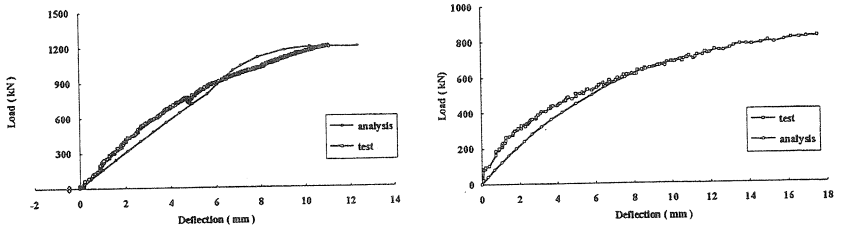

(a) Wall W4 (b) Wall W9

Fig. 5 Relative deflection of two points for Group 3 (e_1/e_2=-1)

FAILURE MODES

A study on the failure patterns was conducted based on the numerical analysis and the test results. For specimens under investigation, failure can be categorized into three groups: the buckling of the whole cavity wall; the material failure; and the buckling of shear connectors.

Buckling of the whole wall

When loading with single curvature and equal eccentricities at the two ends of specimen, failure, in most instances, was the buckling of the whole cavity wall. Specimens experienced such failure type underwent a nonlinear deflection stage before load reached the ultimate value as represented by a part of smooth curve in the load-deflection curves. Such nonlinearity were due to the nonlinear constitutive relationships of materials and the slenderness effect. In most cases, the post-buckling strength of the specimen could be traced using stroke control technique in the test or Riks solution method in the analysis.

For specimens loaded with eccentricity only at one end, the failure mode was also the buckling of the whole specimen. Since the maximum moment was at one end of the wall, the slenderness effect might not be as obvious as in the first case where eccentric loads were added at both ends of specimens.

Material failure

The material failure mode happened under a double curvature loading condition. Since the maximum moment occurred at the two ends of the specimen, slenderness effect was not significant. The failure was brittle with a sudden spalling of the face-shell at the top masonry block. No descending part of curve was obtained from the test nor from the analysis. It was detected from the analysis that at the failure zone, concrete block reached the compression strength obtained from the concrete masonry prism tests.

Buckling of the shear connector

In the analysis of specimen W8, it was found that some shear connectors reached their ultimate load capacity and buckled. The buckling started at first layer of connectors from the top of the wall at a load level of 120 kN. More connectors (the second layer from the top and the first layer from the bottom) buckled as the load increased until the whole specimen reached the ultimate load. During the test, although no buckling of the shear connectors was captured due to the difficulty of observation, it was observed that several big cracks formed at veneer causing the wythe of veneer being separated into several rigid parts before reaching the ultimate load. Summarizing the observation from the test as well as from the analysis, it is believed that for the wall with designed shear connector pattern and large eccentricity, $e=t/2$, buckling of shear connectors accompanied with cracking through of the veneer resulted in plastic hinges formed at the locations of cracks in the veneer. The veneer seceded from resisting the moment after the formation of plastic hinges causing the redistribution of the moment among the two wythes of the cavity wall. Because of the existence of reinforcement in the block wythe, the wall could sustain significant load even after reaching the ultimate load.

CONCLUSIONS

It can be concluded that the numerical simulation of masonry cavity wall tests is quite satisfactory. Table 3 summarizes the analytical results for P_u and their comparison to the test results. The average of the ratio $P_{u\ analytical} / P_{u\ test}$ is 1.0170 (or 1.0602 if use average material property for specimen W3). The standard deviation is 0.0835 (or 0.1527 if use average material property for specimen W3).

REFERENCES

Atkinson, R.H. and Yan, G.G. (1990), Results of a Statistical Study of masonry Deformability, Journal of the Masonry Society, Vol. 9, No.1.

Essawy, A.S., Drysdale, R.G. and Mirza F.A. (1985), Nonlinear Macroscopic Finite Element Model for masonry Walls, New Analysis Techniques for Structural Masonry, Proceedings of a Session held in conjunction with Structural Congress' 85, Illinois.

Goyal, A., Hatzinikolas, M.A. and Warwaruk, J., (1993), Shear Connected Cavity Walls Under Vertical Loads, Structural Engineering Report No. 182, Dept. of Civil Engineering, University of Alberta, January, 1993.

Hibbitt, Karlsson and Sorensen, (1994), ABAQUS User's Manuals, Version 5.3, Hibbitt, Karlsson and Sorensen Inc., Providence, RI.

Lotfi, H.R., Hamid, R., Shing, P.B. and Benson, (1994), Interface Model Applied to Fracture of Masonry Structures, ASCE Journal of Structures, Vol. 120 No.1, pp 63-80.

Papanikolas, P.A., Hatzinikolas, M.A., Warwaruk, J. and Elwi, A.E. (1989), Experimental and Analytical Results for Shear connected Cavity Walls, 5th Canadian Masonry Symposium, Department of Civil Engineering, University of British Columbia, Vancouver, B.C.

Wang, R. Elwi, A.E., Hatzinikolas, M.A. and Warwaruk, J. (1995), Tests of Tall Cavity Walls Subjected to Eccentric Loading, Proceedings of the Seventh Canadian Masonry Symposium, Hamilton, Ontario.